Preprocessing of Hyperspectral Images - a Comparative Study of Destriping Algorithms for EO-1 Hyperion

Daniel Scheffler*[a], Pierre Karrasch[b]
[a]GFZ German Research Centre for Geosciences, Telegrafenberg, 14473 Potsdam, Germany;
[b]Professorship of Geoinformation Systems, Technische Universität Dresden, Helmholtzstraße 10. 01069 Dresden, Germany

ABSTRACT

In this study, data from the EO-1 Hyperion instrument were used. Apart from atmospheric influences or topographic effects, the data represent a good choice in order to show different steps of the preprocessing process targeting sensor-internal sources of errors. These include the diffuse sensor noise, the striping effect, the smile effect, the keystone effect and the spatial misalignments between the detector arrays. For this research paper, the authors focus on the striping effect by comparing and evaluating different algorithms, methods and configurations to correct striping errors. The correction of striping effects becomes necessary due to the imprecise calibration of the detector array. This inaccuracy affects especially the first 12 visual and near infrared bands (VNIR) and also a large number of the bands in the short wave infrared array (SWIR). Altogether six destriping techniques were tested on the basis of a Hyperion dataset covering a test site in Central Europe. For the final evaluation, various analyses across all Hyperion channels were performed. The results show that some correction methods have almost no effect on the striping in the images. Other methods may eliminate the striping, but analyses show that these algorithms also alter pixel values in adjacent areas which originally had not been disturbed by the striping effect.

Keywords: Hyperspectral, preprocessing, destriping, Hyperion, EO-1

1. INTRODUCTION

In the last decades, especially the geometric resolution of satellite and airborne remote sensing systems increased significantly. The importance to detect small-scale geometric details forms the basis of a wide range of applications dealing with remote sensing data. In addition to this development the spectral resolution of the systems has also been improved. While multispectral systems are mainly characterized by discrete spectral bands, hyperspectral systems are mainly distinguished by the fact that they close the remaining gaps in the solar spectrum to provide a quasi-continuous signal of the earth's surface.

Until the late 1980s, hyperspectral remote sensing was considered as a new scientific development. Their potential for a purposeful detection of certain materials was recognized at an early stage [1]. Primarily organizations such as the NASA or the U.S. Army fostered a decisive drive in research [2-6]. With the completion of the first airborne hyperspectral sensor "Airbourne Imaging Spectrometer" (AIS) in 1984, developed by the Jet Propulsion Laboratory (JPL), the NASA responded to the former needs for research for the development of high spectral resolution remote sensing sensors. This instrument with already 128 spectral bands in the range of 900 nm to 2400 nm [5] has been further developed. Since the 1987 it is known as the "Airbourne Visible/Infrared Imaging Spectrometer“ (AVIRIS) and is still working today. With 224 spectral bands (10 nm bandwidth) between 410 nm and 2450 nm and a ground sampling distance of 4 m [7] the requirements for the monitoring of the earth's surface by means of hyperspectral remote sensing techniques were fulfilled. Corresponding early scientific projects were described in [8-10]. The development of numerous other airborne spectrometer systems such as DAIS-7915 (1995), HYDICE (1994), HyMap (1998), HySpex (2003) or AHS (2004) leads to a gain in importance of hyperspectral remote sensing.

With Hyperion, the NASA started the first spaceborne hyperspectral sensor. Since that time Hyperion is one of three instruments of the Earth Observing-1 satellite with similar specification as AVIRIS. With this instrument it was possible

*daniel.scheffler@gfz-potsdam.de; phone +49 331 288-1764; fax +49 331 288-1192; www.gfz-potsdam.de

Image and Signal Processing for Remote Sensing XIX, edited by Lorenzo Bruzzone,
Proc. of SPIE Vol. 8892, 88920H · © 2013 SPIE · CCC code: 0277-786X/13/$18
doi: 10.1117/12.2028733

to broaden the field of application. Particularly the authors Fred A. Kruse, Joseph W. Boardman und Jonathan F. Huntington could show how Hyperion data can help to find answers to geological and mineralogical issues [11-14]. Other studies used Hyperion data for remote sensing of vegetation [15-18], soils [19,20] and the atmosphere [21,22]. This demonstrates the significant potential of hyperspectral remote sensing data in the application to spectrally similar objects.

What all of those applications have in common is the need of a highly accurate calibration. Already in the 1980s, Gross & Klemas [5] carried out basic research into the preprocessing and radiometric calibration of hyperspectral imagery as an essential foundation in the use of this then newly developed data source. Methods for radiometric correction are usually based on calibration and validation measurements carried out in the laboratory prior to or directly after the launch of a newly developed sensor. That applies to Hyperion, too [23,24]. Along with the launch of Hyperion, a lot of studies on the further development of preprocessing techniques have been published. Studies including the radiometric calibration have been carried out [23-26]. Extensive approaches for the preprocessing of Hyperion data considering the known distortions were published by an Australian research team belonging to the CSIRO Earth Observation Centre [27-29]. Furthermore in [30-35], particularly with regard to the correction of image stripes and the smile effect, the authors Datt et al. [31] und Goodenough et al. [32] made an important contribution.

It is becoming clear that there are different approaches available for the preprocessing of Hyperion data. On the other hand it shows that no standardized preprocessing algorithm exists. The goal of this study is, besides an overview of different radiometric effects on Hyperion data (section 2) and an introduction to the preprocessing workflow of Hyperion data, to focus on the striping effect and the different available algorithms for elimination of these artifacts. For this reason, altogether six different methods will be introduced (section 4.2) and analyzed on the basis of different criteria (section 5.1). Finally, the author will give some recommendations referring to the analyzed destriping algorithms (section 5.3).

2. RADIOMETRIC EFFECTS ON REMOTE SENSING DATA

To recognize the need for the preprocessing of hyperspectral imagery, it is essential to understand possible radiometric effects on remote sensing data. A significant influence to radiometric measurements in the field of remote sensing is the presence of atmospheric disturbances to the electromagnetic radiation while passing through the atmosphere. Effects of absorption and scattering could modify the signal. Depending on the material composition of the atmosphere, the resulting changes also differ in accordance with the observed wavelength. For this reason, the atmospheric footprint on remote sensing data has to be considered if spectral characteristics comparable to ground measurements are needed for further investigations.

A second field of radiometric effects on remote sensing data arises due to the morphology of the earth surface and is comparable with the influence of the atmosphere. Variable angles of reflection or effects of shadowing could also have an influence to the spectral signature of surface objects.

In addition to the previously described factors there are some further sensor internal effects which have an impact on the radiometry of the data. Sensor noise is certainly one of the most important sensor internal effects in remote sensing data. The CCD detector elements are set in a higher state of charge according to the incident energy of radiation. At the same time varying materials of the detectors can lead to different sensitivities to this radiation. If differences in the calibration of the sensors exist, or temperature differences occur, the noise of the sensor can increase [36]. Due to the principle of the data acquisition it is possible that artifacts, such as stripes in the images, disturb the visual impression. In addition it must be considered that in general the sensitivity of the detectors decrease over the time of operation. This can lead to a shift of the center position of the spectral channels [37,38].

The so-called smile effect is another sensor internal effect, which occurs mainly in hyperspectral sensors like Hyperion. The radiation which is split at the diffraction grating is projected onto the detector. This can lead to aberrations in form of a spectral distortion of the image information [39,40]. Thereby the centre of the spectral bands shifts a few nanometers, possibly in addition to a change of the bandwidth. The amount of these spectral shifts varies from band to band and in cross-track direction [28,32], which makes a correction complicated. For a detailed analysis of the spectral signatures in hyperspectral images, the precise correction of this effect is essential.

The so-called keystone effect as well as the smile effect is caused by aberrations or slight misalignments of the optical components in the sensor system. The keystone effect is expressed as a spatial displacement perpendicular to the flight

direction (cross-track) of the sensor. Its amount depends on the column and the band number [41]. This means that the recorded objects are not exactly at the same spatial position in every available band. The maximum shift for Hyperion data is 0.5 pixels [42].

For technical reasons it does not seem to be possible to detect the whole solar spectrum with a single detector. Therefore many remote sensing systems consist of two or more spectrometer systems, which usually leads to co-calibration / -registration issues. For example Hyperion uses different algorithms for the readout of the data acquired by both spectrometers. This procedure causes a small time difference and leads to a spatial shift of one pixel between the two Hyperion detector arrays [43].

3. PREPROCESSING OF HYPERION DATA

3.1 Hyperion – Used Data Set

The Hyperion sensor is one of in total three instruments on NASA´s EO-1 satellite that has been launched in 2000. Being a typical pushbroom sensor, Hyperion acquires hyperspectral satellite data with a 30 m ground sampling distance (GSD) and provides 242 spectral bands between 356 nm and 2577 nm (198 bands exposed due to low SNR) at a spectral resolution of 10 nm. The instrument consists of two imaging spectrometers and therefore two separate detector arrays with altogether nearly 62,000 detector elements. The VNIR spectrometer records 70 bands below 1058 nm and the SWIR spectrometer 172 bands above 852 nm. One simultaneously recorded scan line (256 px) covers an approx. 7.7 km wide area on the ground while the scene length varies between 42 km and 185 km. The average signal to noise ratio (SNR) ranges from 161:1 (VNIR) to 40:1 (SWIR) [24]. Acquisitions are carried out on demand with a maximum repetition rate of 14 days. The data can be downloaded at no charge from the USGS servers since 2009 [44].

This study is based on an off-nadir acquisition covering a test site in the central European region (East Germany) that consists of a mixture of agricultural land, forests, urban areas, water surfaces and an opencast mining area. The specifications of the scene are summarized in Table 1.

Table 1. Specifications of the used Hyperion data set.

Parameter	Value
Scene-ID	EO1H1940242012145110KF_SGS_1
Preprocessing Level	L1R
Acquisition date / time (UTC)	24.05.2012 / 09:59:49 - 10:04:08
Sensor look angle	19.52°
Geographical extent	NE: 52.20°N / 12.18°E SW: 51.41°N / 11.63°E (7.7 km x 96 km)
Cloud coverage	0 %

The used Level 1R data (HDF file format) already have undergone some preprocessing steps performed by the USGS prior to the publication. This so-called Level 1 Preprocessing includes the solar / dark calibration, smear correction, echo removal and a correction of obviously bad pixels [45]. Georeferencing of the data is not included which facilitates preprocessing steps like a destriping or the correction of the smile effect. The delivered Level 1R (L1R) data represent radiance at sensor measurements that have been scaled to digital numbers using the factors 400 (VNIR) and 800 (SWIR).

3.2 Preprocessing workflow

Figure 1 shows a possible workflow for the preprocessing of the hyperspectral satellite data acquired by Hyperion. This workflow turned out to be reasonable as a result of this study while it includes all relevant corrections in the case of Hyperion L1R data. The order of the particular preprocessing steps has been chosen in a way that ensures a minimal

alteration of the valuable hyperspectral image information whereas every step produces an optimal data base for the following one. For example, an atmospheric correction cannot lead to accurate results prior to the correction of sensor-internal errors like spectral or spatial misalignments or inaccurate detector calibrations. A resampling as part of a georeferencing or an orthorectification alters the image information and should be performed (if necessary) after an atmospheric correction. Similar preprocessing workflows in the context of Hyperion have been published by the authors Staenz et al. [30], Khurshid et al. [33] and Hitchcock & White [34].

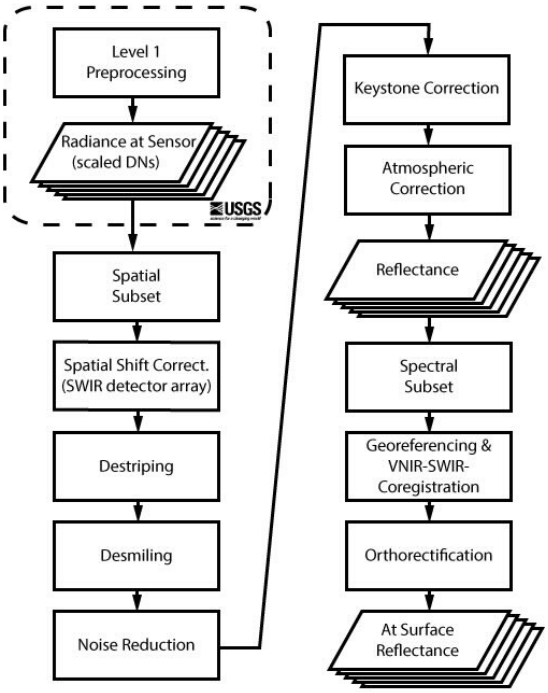

Figure 1. Preprocessing workflow for hyperspectral satellite data of the sensor EO-1 Hyperion.

This paper is focused on the evaluation of various destriping techniques as an important part of the Hyperion preprocessing workflow.

4. STRIPING EFFECT

4.1 Background - Striping

Hyperion L1R data show a severe striping effect that is caused by an inaccurate co-calibration (see section 2) of the individual detectors on the focal plane array (FPA). Since each Hyperion detector records a whole image column inside of a particular spectral band, the amount of striping varies as a function of wavelength and column number corresponding to the detector position on the two-dimensional FPA. Especially the first 12 visual and near infrared (VNIR) bands and also a large number of the bands in the short wave infrared array (SWIR) are affected. Previous analyses show that for Hyperion data detector error standard deviations of up to 123 DN can be expected in the shortest wavelengths of the SWIR array (representing about 2 % of the global mean) [46].

It is evident that an uncorrected striping effect will lead to faulty interpretation results of the data. This is particularly applicable to research projects where a high similarity of relevant signatures exists. Therefore, a destriping technique should be applied that provides optimal results in both the removal of the image stripes and the preservation of the original spectral information.

4.2 Destriping Algorithms

Since every image column per band corresponds to the signal of the same Hyperion detector (prior to any resampling), the adjustment of the individual column statistics is possible in order to destripe the data. Such methods are based on global or local statistic algorithms implying that each individual column mean and/or standard deviation is equaled to the global mean of the spectral band or to the statistics of adjacent columns. Other methods rely on a transformation of the dataset into the frequency domain and use the amplitudes of each image row to find and eliminate significant variations. Some destriping techniques adjust only predefined image columns, other methods use a threshold to identify image columns that have to be corrected, other ones cause a recalculation of the whole image information.

In this study altogether six destriping techniques were tested on the basis of the above mentioned Hyperion dataset:

1. *Destriping based on ENVI Hyperion Tools:* The ENVI-plugin Hyperion-Tools features a method called "Flag Mask Correction" offering a local-statistic algorithm which performs a simple linear interpolation between adjacent image columns. It is based on a predefined "Flag Mask" that determines a few specific columns (stripes) per band in order to recalculate their pixel information [47].
2. *Destriping based on ENVI-SPEAR-Tools – Vertical Stripe Removal:* This method is also implemented in ENVI but only inadequately described in publications or manuals. However, an advantage may be the option to exclude certain areas from the corrections, e.g. very bright (mostly clouds) or very dark image areas.
3. *Destriping based on ENVI General Purpose Utilities – "Destripe":* Another ENVI implemented method which originally has been developed for the Landsat-MSS-sensor. Under certain conditions, this global-statistic algorithm is also applicable to Hyperion data. Since the algorithm is designed to correct horizontal image stripes, Hyperion datasets have to be rotated by 90 degrees prior to the destriping process.
4. *Destriping based on a method by Datt et al. (2003) [31]:* This local-statistic approach analyses the mean and standard deviation of columns in a user defined window (filter width). If these parameters exceed a given threshold, a recalculation of the relevant column is carried out which equals the column statistics to the median of all column means and column standard deviations inside the filter kernel. The algorithm has been implemented through a MATLAB script.
5. *ERDAS Periodic Noise Removal:* This approach is part of the ERDAS Imagine Software package and was developed for the correction of periodical noise in the images. It uses a fourier transformation to analyze the dataset in the frequency domain [48].
6. *Destriping using Wavelet Fourier Adaptive Filtering (WFAF) based on algorithm by Pande-Chhetri & Abd-Elrahman (2011; 2012) [49,50]:* This algorithm is designed to correct non-periodic image stripes without a significant alteration of the spectral information. It is based on a combination of wavelet decomposition and frequency domain adaptive filtering. The image is decomposed into several wavelet components with different scale levels that can be used to extract certain components with a notable direction (corresponding to image stripes). These are transformed into the frequency domain where the vertical component can be removed using an adaptive filter [49,50]. The algorithm can be applied directly to the image data (in the image domain) or in the frequency domain after a minimum noise fraction (MNF) transformation. In this study the algorithm (provided as a MATLAB script by the authors) has been adopted to Hyperion in order to destripe all of the 242 Hyperion bands separately. Both approaches have been tested whereby it turned out that an interpolation of extremely deviating columns (e.g. dead detectors) is reasonable to be performed prior to the WFAF-algorithm.

All methods have been applied to the whole Hyperion dataset in its original geographical extent. This minimizes the effect of extremely bright or dark image regions onto the local column statistics which would otherwise possibly lead to artifacts inside of the destriping result.

The used input parameters for each evaluated destriping algorithm are listed in Table 2:

Table 2. Used Input Parameters for destriping.

Destriping technique	**Used Input Parameters**
ENVI Hyperion Tools [47]	standard flag mask (predefined)
ENVI-SPEAR-Tools – Vertical Stripe Removal	darkest 10 % and brightest 5 % of band 8 masked
ENVI General Purpose Utilities – Destripe	number of detectors: 256
Local Destriping [31]	filter width: 21 columns, 41 columns threshold: 0.1
ERDAS Periodic Noise Reduction [48]	minimum affected frequency (MAF): 5, 50, 90
Wavelet-based destriping [49,50]	wavelet type: db4 decomposition levels: 4 (static for all bands) threshold value k: 1
MNF-Wavelet-based destriping [49,50]	processed MNF bands: 1 - 10 wavelet type: db4 decomposition levels: 2, 3, 3, 5, 5, 6, 6, 7, 8, 8 (dynamic) threshold value k: 1

5. EVALUATION

5.1 Evaluation criteria and results

Three main criteria were used to assess the quality of the different destriping algorithms.

- total number and positions of corrected image columns
- the amount of alteration to the sensor's initial signal
- visual impression

Fig. 2 shows the positions of the corrected image columns per spectral band and provides an overview of the number of the recalculated image information in the whole Hyperion dataset. Each image column that has been recalculated during the destriping process is represented by one black dot. The bands 1-7, 58-76 and 225-242 have no corrected stripes because these bands do not contain any image signal. Their spectral information has been deleted during the USGS Level 1 Preprocessing due to the low SNR of the Hyperion sensor in these wavelength regions [45].

The amount of alteration to the initial signal of the sensor cannot be seen in Fig. 2. For that purpose the plots in Fig. 3 have been calculated. The plotted column means have been calculated from the original digital numbers as well as from each destriping result (smoothed to provide a better graphic representation using a mean filter with 10 columns as filter width). They can be utilized in the evaluation of the above mentioned destriping techniques when assessing their ability to remove image stripes without a significant alteration of the spectral information. Small-scale variations of the plotted column means are mostly related to image stripes. Hence an ideal destriping technique should be able to eliminate them.

A qualitative / visual assessment of the various destriping techniques can be derived from Fig. 4 where the correction results are shown at the example of a Hyperion band 8 subsample (427 nm). The differential images between the original imagery and the destriping result (destriped minus original) are each shown below, indicating the position of change.

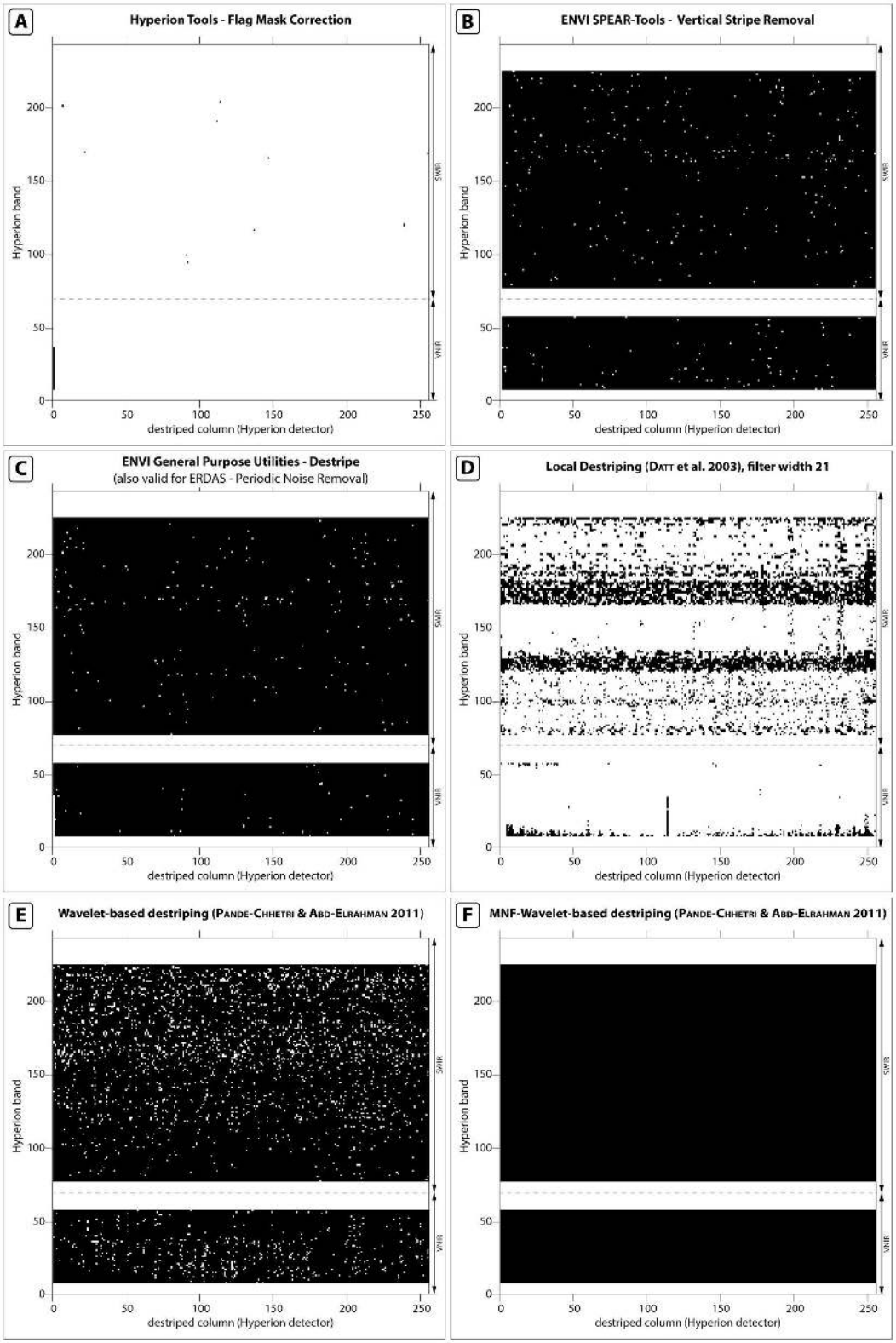

Figure 2. Positions of the modified image columns depending on the applied destriping technique.

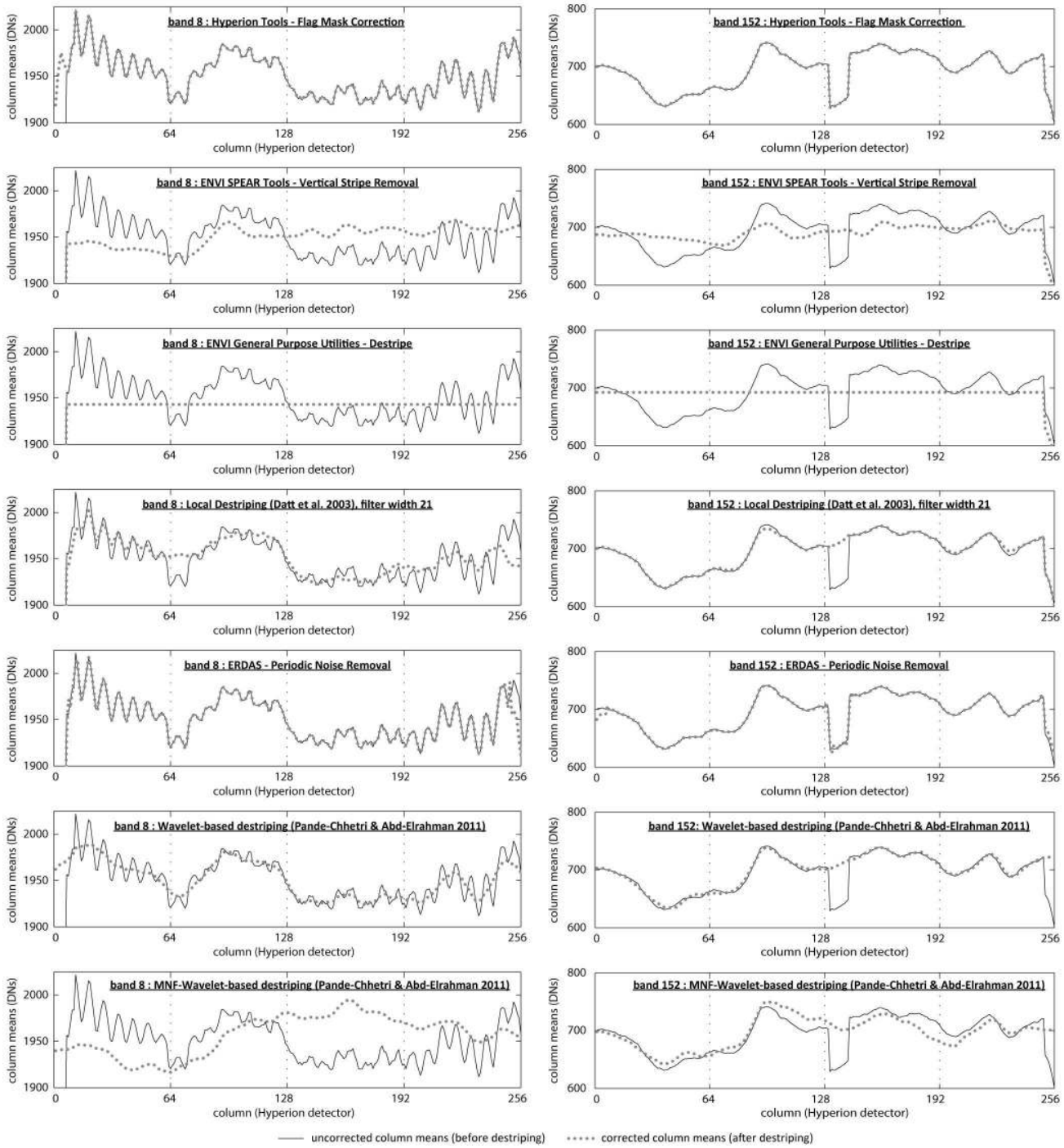

Figure 3. Column means of band 8 (427 nm) and 152 (1670 nm) before and after the tested destriping techniques.

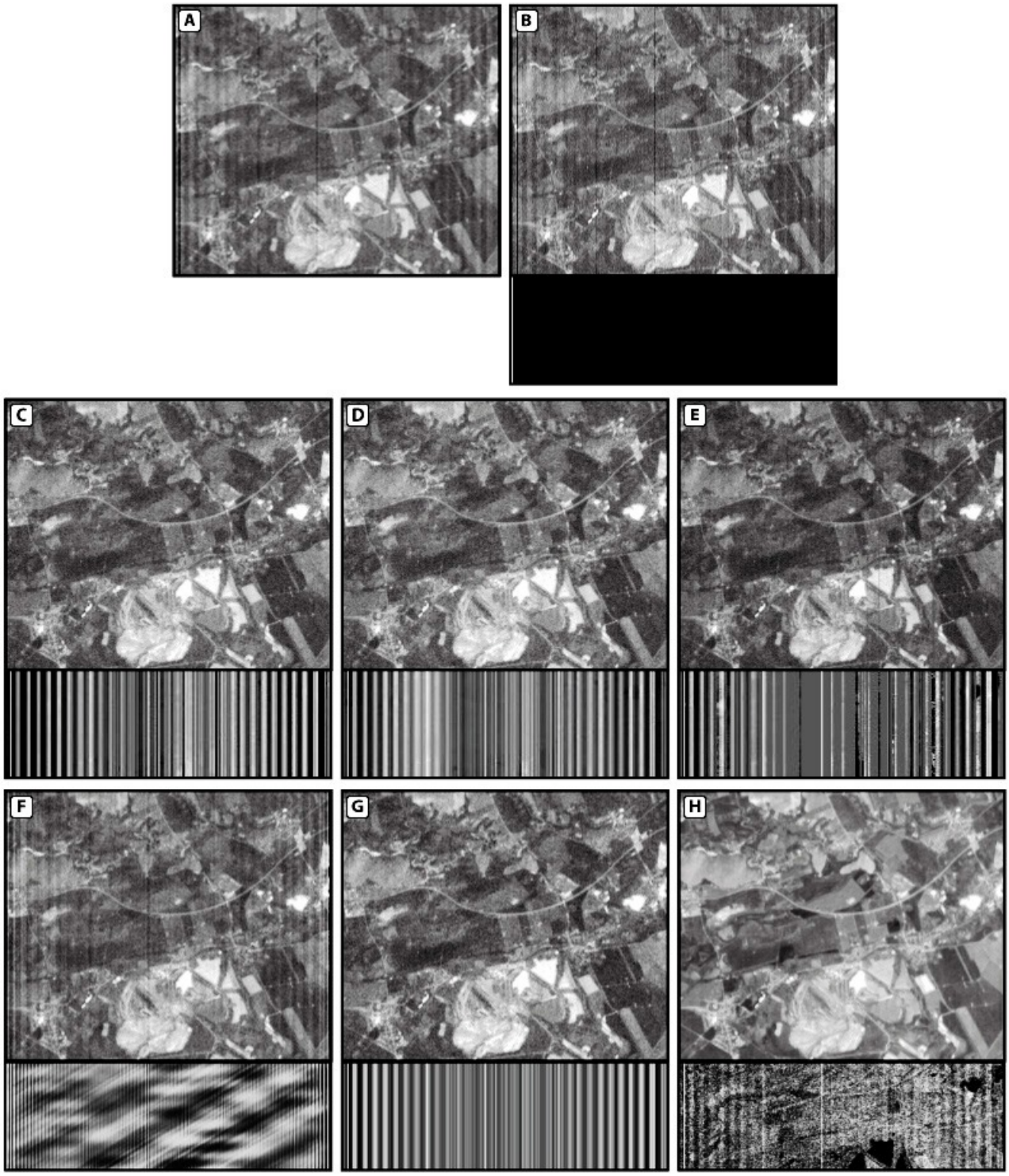

Figure 4. Destriping results depending on the destriping technique with the corresponding differential image below each. (A) uncorrected L1R data; (B) Hyperion Tools – Flag mask correction; (C) ENVI-SPEAR-Tools - Vertical Stripe Removal; (D) ENVI General Purpose Utilities – Destripe; (E) Local Destriping, filter width of 21 columns; (F) ERDAS Periodic Noise Removal (MAF 50); (G) Wavelet Fourier Adaptive Filtering, image domain; (H) Wavelet Fourier Adaptive Filtering, MNF domain

5.2 Discussion

The methods “Flag Mask Correction“ (Hyperion Tools) and “ERDAS Periodic Noise Removal“ do not show significant changes after the destriping procedure. Judging from the visual impression, all other algorithms result in significantly better results (Fig. 4).

Fig. 2 confirms the minimal effect of “Flag Mask Correction“. Only a few predefined columns out of the whole image cube have been recalculated. The remaining image information keeps unaffected. Correspondingly, Fig. 3 shows only changes in such column positions that have been marked as image stripes through the flag mask. In this case this only applies to column 1 (band 8, 427 nm) which can also be seen in the difference image in Fig. 4. Hence this destriping algorithm is not recommended for the removal of the strong striping effect of Hyperion as long as the underlying flag mask is not edited by the user manually. However, a manual adjustment of the flag mask would be very time-consuming in consideration of the nearly 200 exposed spectral bands of Hyperion.

Although the destriping algorithm “ERDAS Periodic Noise Removal“ (frequency based) recalculates the whole image information in all spectral bands and image columns (Fig. 2 C), the difference to the uncorrected L1R data is marginal (see Fig. 3). This is related to the fact that this algorithm has been designed to remove image stripes occurring at regular intervals [48] whereas Hyperion data only contain non-periodic stripes due to the sensor´s pushbroom acquisition system. Therefore the difference image in Fig. 4 cannot support a reasonable destriping result in comparison with the real striping patterns of the data. In fact the whole hyperspectral image data is affected in regular patterns (Fig. 4), which don’t even match the vertical direction of the Hyperion image stripes. For that reason it can be assumed that the “ERDAS Periodic Noise Removal“ cannot lead to improvements of the image information acquired by a pushbroom system. The three different configurations that have been tested during this study (maximum affected frequency: 3, 50 and 90) did not show remarkable differences between each other.

The destriping techniques “ENVI SPEAR-Tools – Vertical Stripe Removal“ and “ENVI General Purpose Utilities – Destripe“ provide – visually evaluated – an almost stripeless result (Fig. 4 C and D). Only dark image regions still show some remaining stripes. Both methods recalculate nearly the whole image information (Fig. 2 B and C). As the analysis has revealed, the global statistic algorithm of the “Destripe”-method causes a vulnerability to extremely bright or dark image regions. For example, in case of a bright image area (clouds etc.) the mean value of the corresponding columns is higher than in the other part of the image. In this case, the equalization of all column means to the global mean of the spectral band causes the affected columns to be assigned lower pixel values which results in a dark block striping (several adjacent dark columns) in the area of those columns. This effect is less significant if the processed dataset has numerous image rows. Hence it is not visible in Fig. 4 as in that case the processed dataset contains more than 3400 rows. The “Vertical Stripe Removal”-technique offers a possibility to exclude such extremely bright or dark image regions (e.g. the darkest or brightest 5 % of the spectral band) from the statistical calculations during the destriping process. This can be seen as an advantage of this method. Despite the nearly stripeless results of both methods (Fig. 4 C and D), the column means in Fig. 3 make clear that the spectral information has been considerably changed in comparison to its original state. Especially if the processed spectral band is dominated by strong cross-track brightness changes, large deviations can be expected. In this study relative deviations of 11.1 % (“Vertical Stripe Removal”) and 12.3 % (“Destripe”) have been measured at the example of Hyperion band 152 (1670 nm). So the “Vertical Stripe Removal”-method leads to minor deviations compared to the “Destripe”-method which sets the same column mean for all columns across the track. However, spectral deviations in this magnitude are not acceptable if a precise interpretation of the spectral information is intended.

The threshold controlled local statistic method “Local Destriping” [31] with a filter width of 21 columns for all bands results in a strong decrease of the Hyperion striping effect (Fig. 3, 4). Nevertheless it does not remove all of the image stripes. In the case of Hyperion band 8 (427 nm), the remaining stripes are mainly concentrated on the left and the right image borders. Fig. 2 confirms that this method only recalculates a small part of the image information which has exceeded the given threshold. In this study only 18.5 % of all image columns in the entire hyperspectral image cube had to be recalculated (at a filter width of 21 columns and a threshold of 0.1). This selective correction can be understood as a great advantage of this destriping method. It enables the algorithm to take corrective action with a strict focus on those parts of the image regions where such correction is necessary. As it can be seen in Fig. 2 the need for a correction depends on the spectral wavelength. The presence of strong water absorption features (bands 120 to 132 – around 1400 nm; bands 165 to 182 – around 1900 nm) is related to a low SNR of the Hyperion sensor which causes a particularly strong striping-effect in those wavelength regions. If the Hyperion SNR is relatively high, far less image columns exceed the threshold so that most of the original spectral information stays unaffected. It can also be seen in Fig. 3 that the

corrected column mean values are relatively close to the original ones (deviations of 2 % in maximum with regard to Hyperion band 8) even though the stripes have not been completely eliminated. Especially the detectors 1 to 50 still show significant variations in the column mean values (Fig. 3) which also can be seen in Fig. 4. This implies that stronger corrections would have been necessary here. Further the analysis of Hyperion band 152 (1670 nm) showed that the algorithm can also correct two adjacent stripes without any problems. Comparing the two filter widths that have been evaluated in this study (Tab. 2) the analysis revealed that a wider filter kernel makes it possible to correct block striping effects more effectively than a narrower one. At the example of band 8 (427 nm) where block stripes occur in the outermost 50 image columns, the standard deviation of the column means could be reduced from 135.1 DNs (uncorrected L1R data) to 124.7 DNs at a filter width of 21 columns and to 122.7 DNs at a filter width of 41.

With regard to Fig. 4 G and H, it is evident that the destriping-algorithm "Wavelet Fourier Adaptive Filtering" [48,49] provides excellent visual results at the configurations that have been tested in this study. It can also be seen in Fig. 4 G and H (especially when assessing the differential images) that the approach working in the MNF domain not only corrects the image stripes (like the one working in the image domain) but also the diffuse sensor noise. This effect is caused by the selection of the first MNF bands containing the highest SNR values during the correction process and it leads to a significant increase of the optical image quality. However, at the same time the MNF approach causes a much higher alteration of the sensor´s initial compared to the approach working directly in the image domain (Fig. 3). This finding applies mainly to those spectral bands that contain a lot of image stripes in the uncorrected state. An example for that is the Hyperion band 8 where the MNF approach leads to deviations of up to 3.8 % in comparison to the original column means (values based on smoothed data). Conversely the approach working in the image domain matches the course trend of the original cross-track column means very well (deviations of 1.8 % in maximum) whereas it also eliminates all of the small-scale variations between the mean values of adjacent columns (corresponding to image stripes). It may be noted that the originally extremely low mean value of column 1 of band 8 is caused by a bad detector signal and had to be corrected prior to the destriping procedure using the "Wavelet Fourier Adaptive Filtering". For this reason, the high deviation to the initial signal in this image column cannot be addressed by the destriping algorithm itself but by separately eliminating extremely divergent image columns. This previously performed correction step was necessary in order to avoid strong artifacts that are caused only by this destriping method in conjunction with a locally bad detector signal (columns with outlying pixel values). Although both approaches of this destriping method lead to a recalculation of nearly the entire image cube (Fig. 2) it was found that a significant alteration of the spectral information takes place only in those image regions that were identified as affected by image stripes.

The ability to perform such target-oriented corrections is one of the main advantages of the "Wavelet Fourier Adaptive Filtering" as well as of the threshold controlled "Local Destriping" or the "Flag Mask Correction".

It is apparent that in case of Hyperion a complete correction of all image stripes can only be reached by an iterative process that includes automatic destriping techniques as well as manual adjustments depending on the nature of the data. For example, the ENVI module "Band Animation" can be used to quickly localize remaining image stripes after the destriping process. Those stripes can then be easily corrected by e.g. the "Flag Mask Correction" tool with the usage of an edited flag mask. In addition, the ENVI module "Spatial Pixel Editor" also offers a possibility to interpolate adjacent image columns manually.

5.3 Final assessment

Besides the above mentioned evaluation criteria other, softer evaluation factors have been considered. Framework conditions such as the workload for pre- and postprocessing, the computational effort and the implementation of the destriping algorithms into available software packages play a decisive role for most users of hyperspectral imagery like those acquired by EO-1 Hyperion.

Table 3 provides an overview of the assessment of the destriping techniques that have been considered in this study.

Table 3. Assessment of the different destriping techniques (scale of assessment: ++, +, 0, -, --).

destriping technique \ criterion		visual impression: correction of image stripes	visual impression: correction of diffuse sensor noise	preservation of the sensor´s initial signal: low SNR	preservation of the sensor´s initial signal: high SNR	percentage of recalculated image columns (whole image cube)	workload (incl. pre- and postprocessing)	computational effort	software implemetation	overall result
ENVI Hyperion Tools - Flag Mask Correction [47]		-	0	++	++	0.08 %	++	++	ENVI	0
ENVI SPEAR-Tools - Vertical Stripe Removal		++	0	-	-	98.6 %	+	0	ENVI	0
ENVI General Purpose Utilities – Destripe		++	0	--	--	99.2 %	0	0	ENVI	0
Local Destriping [31]	filter width 21	+	0	++	++	18.5 %	++*	0	MATLAB	+
	filter width 41	+	0	++	++	23.0 %	++*	0	MATLAB	+
ERDAS - Periodic Noise Removal [48]	MAF 3	--	0	+	+	100 %	-	--	ERDAS	-
	MAF 50	--	0	+	+	100 %	-	--	ERDAS	-
	MAF 90	--	0	+	+	100 %	-	--	ERDAS	-
Wavelet Fourier Adaptive Filtering [49,50]	directly in the image domain	++	0	++	++	94.6 %	+*	-	MATLAB	++
	MNF-domain	++	++	0	+	100 %	+*	0	MATLAB	++

* The assessment applies to the MATLAB-codes that have been programmed as a part of this study.

Thereby the ratings "++" and "+" represent a high and a moderate improvement of the initial situation (Level 1R), respectively. "0" marks methods without noticeable change and "-" or "--" indicate moderate and high deterioration, respectively. A high workload or computational effort has been marked as "--".

As a result of this study, the destriping technique "Flag Mask Correction" (ENVI-plugin Hyperion Tools) cannot be recommended without an accurate modification of the default flag mask due to its insufficient correction. The "Periodic Noise Removal" (ERDAS Imagine) is also not suitable to correct Hyperion image stripes because of their non-periodic pattern. The ENVI modules "Vertical Stripe Removal" (SPEAR Tools) and "Destripe" (General Purpose Utilities) lead to a nearly complete removal of the image stripes whereby the former one is able to prevent artifacts in case of a small image size (few image rows) in combination with extremely bright or dark image regions. However, these techniques lead to a significant alteration of the initial sensor signal. The "Local Destriping" proposed by Datt et al. [31] largely preserves the original spectral information but the analysis showed that the usage of only one single filter width cannot remove the whole striping effect. Nevertheless, it is easy to use and can be recommended as a fast and effective destriping method for Hyperion data. The "Wavelet Fourier Adaptive Filtering" working in the MNF-domain provides the visually best destriping result in comparison with the other methods tested here and it also includes a noise reduction. However, it has also been evaluated as a method leading to a considerable amount of alteration to the sensor´s initial signal. The same method but applied directly in the image domain provides a stripeless result and preserves the original image information very well. For that reason the Wavelet Fourier Adaptive Filtering [49,50] being applied in the image domain can be highly recommended in order to completely destripe Hyperion data with a special focus on the preservation of the valuable hyperspectral image information. However, it should be noted that a correction of extreme image columns (according to a given threshold) has to be performed previously to prevent artifacts.

6. SUMMARY / CONCLUSION

The goal of the presented comparative study was to facilitate the workflow of the preprocessing of hyperspectral Hyperion data. For this purpose, an analysis of the whole procedure of preprocessing as well as a classification of the individual operation of destriping has been carried out. The analysis of the presented methods was based on different criteria. The analysis demonstrates that the quality of the various available methods is very different. Further potential for improving the destriping process is mainly seen in the various settings of the Adaptive Wavelet Fourier filtering.

Finally it must also be mentioned that the quality of the preprocessing of Hyperion data is not predictable only on the basis of the quality of the destriping. Rather it is necessary that all steps of the preprocessing process were involved in the quality assessment as shown in section 3. In case of Hyperion data this applies particularly to the elimination of radiometric effects due to the smile effect. Using the results presented in this study, the user of Hyperion data will be able to estimate the mode of action of different destriping methods as part of the entire process of preprocessing.

ACKNOWLEDGEMENTS

The Hyperion L1R data were processed and provided by the USGS. We thank Devin White, Roshan Pande-Chhetri and Amr Abd-Elrahman for their support and for making their program codes available for our studies.

REFERENCES

[1] Goetz, A.F.H., Rowan, L.C., "Geologic remote sensing," Science 228:781-791 (1981).
[2] Goetz, A.F.H., "High spectral resolution remote sensing of the land," SPIE 475 Remote Sensing: 56-68 (1984).
[3] Goetz, A.F.H., Vane, G., Solomon, J.E., Rock, B.N., "Imaging Spectrometry for Earth Remote Sensing," Science 228(4704): 1147-1153 (1985).
[4] LaBaw, C., "Airborne Imaging Spectrometer. An advanced concept instrument," Proceedings of SPIE 0430, Infrared Technology IX: 68-74 (1984).
[5] Gross, M.F., Klemas, V., "The use of Airborne Imaging Spectrometer (AIS) data to differentiate marsh vegetation," Remote Sensing of Environment 19: 97-103 (1986).
[6] Rinker, J.N., "Hyperspectral Imagery, A New Technique for Targeting and Intelligence," Presented at the Army Science Conference, Durham, NC: 1-16 (12-15 June 1990).
[7] Porter, W.M., Enmark, H.T., "A system overview of the Airborne Visible/Infrared Imaging Spectrometer (AVIRIS)," Proceedings of SPIE 834: 3-12 (1987).
[8] Roberts, D.A., Smith, M.O., Adams, J.B., "Green vegetation, nonphotosynthetic vegetation, and soils in AVIRIS data," Remote Sensing of Environment 44: 255-269 (1993).
[9] Gao, B.C., Heidebrecht, K.B., Goetz, A.F.H., "Derivation of scaled surface reflectances from AVIRIS data," Remote Sensing of Environment 44(2–3):165–178 (1993).
[10] Boardman, J.W., Kruse, F.A., Green, R.O., "Mapping target signatures via partial unmixing of AVIRIS data," 5th Annual JPL Airborne Earth Science Workshop, Jet Propulsion Laboratory Publications 1: 23-26 (1995).
[11] Kruse, F.A., Boardman, J.W., Huntington, J.F., "Comparison of EO-1 Hyperion and Airborne Hyperspectral Remote Sensing Data for Geologic Applications," Proceedings of the IEEE Aerospace Conference, Big Sky, Montana: 3-1501–3-1513 (9-16 March 2002).
[12] Kruse, F.A., Boardman, J.W., Huntington, J.F., Mason, P., Quigley, M.A., "Evaluation and Validation of EO-1 Hyperion for Geologic Mapping," Proceedings of the International Geoscience and Remote Sensing Symposium, 2002, Toronto, Canada: 593-595 (24-28 June 2002).
[13] Kruse, F.A., Boardman, J.W., Huntington, J.F., "Comparison of Airborne Hyperspectral Data and EO-1 Hyperion for Mineral Mapping," IEEE Transactions on Geoscience and Remote Sensing 41(6): 1388-1400 (2003).
[14] Kruse, F.A., "Mineral Mapping with AVIRIS and EO-1 Hyperion," Proceedings of the 12th JPL Airborne Geoscience Workshop, Pasadena, California: 149−156 (2003).
[15] Gong, P., Pu, R., Biging, G.S., Larrieu, M.R., "Estimation of Forest Leaf Area Index Using Vegetation Indices Derived From Hyperion Hyperspectral Data," IEEE Transactions on Geoscience and Remote Sensing 41(6): 1355-1362 (2003).
[16] Thenkabail, P.S., Enclona, E.A., Ashton, M.S., Legg, C., De Dieu, M.J., "Hyperion, IKONOS, ALI, and ETM+ sensors in the study of African rainforests," Remote Sensing of Environment 90: 23-43 (2004).
[17] Huete, A.R., Kim, Y., Ratana, P., Didan, K., Shimabukuro, Y.E., Miura, T., "Assessment of Phenologic Variability in Amazon Tropical Rainforests Using Hyperspectral Hyperion and MODIS Satellite Data," (2008) In Kalacska, M., Sanchez-Azofeifa, G.A., Ed., "Hyperspectral Remote Sensing of Tropical and Subtropical Forests," Taylor & Francis, Boca Raton (2008).
[18] Vyas, D., Krishnayya, N.S.R., Manjunath, K.R., Ray, S.S., Panigrahy, S., "Evaluation of classifiers for processing Hyperion (EO-1) data of tropical vegetation," International Journal of Applied Earth Observation and Geoinformation 13: 228-235 (2011).

[19] Gomez, C., Rossel, R.A.V., Mcbratney, A.B., "Soil organic carbon prediction by hyperspectral remote sensing and field VIS-NIR spectroscopy: An Australian case study," Geoderma 146(2008): 403–411 (2008).
[20] Ghosh, G., Kumar, S., Saha, S.K., "Hyperspectral Satellite Data in Mapping Salt-Affected Soils Using Linear Spectral Unmixing Analysis," Journal of the Indian Society of Remote Sensing 40(1): 129-136 (2011).
[21] Chudnovsky, A., Ben-Dor, E., Kostinski, A. B., Koren, I., "Mineral content analysis of atmospheric dust using hyperspectral information from space," Geophysical Research Letters 36(L15811): 1-5 (2009).
[22] Chudnovsky, A., , Kostinski, A. B., Herrmann, L., Koren, I., Nutesku, G, Ben-Dor, E., "Hyperspectral spaceborne imaging of dust-laden flows: Anatomy of Saharan dust storm from the Bodélé Depression," Remote Sensing of Environment 115(2011): 1013–1024 (2011).
[23] Jarecke, P., Yokoyama, K., "Radiometric calibration of the Hyperion imaging spectrometer instrument from primary standards to end-to-end calibration. Proceedings Optical Science and Technology Symposium, Earth Observing Systems V, SPIE 1435: 1-9 (2000).
[24] Folkman, M., Pearlman, J., Liao, L., Jarecke, P., "EO-1/Hyperion hyperspectral imager design, development, characterization, and calibration," Proceedings of SPIE 4151, Hyperspectral Remote Sensing of the Land and Atmosphere: 40-51 (2001).
[25] Barry, P.S., Shepanski, J., Segal, C., "Hyperion on-orbit validation of spectral calibration using atmospheric lines and on-board system," Proceedings of SPIE 4480: 231-235 (2002).
[26] Kerola, D.X., Bruegge, C.J., Gross, H.N. Helmlinger, M.C., "On-Orbit Calibration of the EO-1 Hyperion and Advanced Land Imager (ALI) Sensors Using the LED Spectrometer (LSpec) Automated Facility," IEEE Transactions on Geoscience and Remote Sensing 47(4): 1244-1255 (2009).
[27] Jupp, D.L.B., "Discussion around Hyperion data," CSIRO Office of Space Science & Applications Earth Observation Centre, Canberra (2001).
[28] Jupp, D.L.B., Datt, B., Lovell, J., Campbell, S., King, E., "Discussions around Hyperion data. Background Notes for the Hyperion Data Users Workshop," CSIRO Office of Space Science & Applications Earth Observation Centre, Canberra (2004).
[29] Datt, B., Jupp, D.L.B., "Hyperion Data Processing Workshop, Hands-On Processing Instructions," CSIRO Office of Space Science & Applications Earth Observation Centre, Canberra (2004).
[30] Staenz, K., Neville, R.A., Clavette, S., Landry, R., White, H.P., "Retrieval of Surface Reflectance from Hyperion Radiance Data," International Geoscience and Remote Sensing Symposium: 1419-1421 (June 2002).
[31] Datt, B., McVicar, T.R., Van Niel, T.G., Jupp, D.L.G., Pearlman, J.S., "Preprocessing EO-1 Hyperion Hyperspectral Data to Support the Application of Agricultural Indexes," IEEE Transactions on Geoscience and Remote Sensing 41(6): 1246-1259 (2003).
[32] Goodenough, D. G., Dyk, A., Niemann, K. O., Pearlman, J. S., Chen, H., Han, T., Murdoch, M., West, C., "Processing Hyperion and ALI for forest classification," IEEE Transactions on Geoscience and Remote Sensing 41(6): 1321-1331 (2003).
[33] Khurshid, K.S., Staenz, K., Sun, L., Neville, R., White, H.P., Bannari, A., Champagne, C.M., Hitchcock, R., "Preprocessing of EO-1 Hyperion Data," Canadian Journal of Remote Sensing 32(2): 84–97 (2006).
[34] Hitchcock, R., White, H.P., "Preprocessing EO-1 Hyperion data using ISDAS," Geomatics Canada, Technical Note 2 (2007).
[35] Kim, W., "Preprocessing of Hyperion," 2011, <http://wonkook.com/home/?page_id=196> (20.11.2012)
[36] Han, T., Goodenough, D. G., Dyk, A., Love, J., "Detection and correction of abnormal pixels in Hyperion images," Proceedings International Geoscience and Remote Sensing Symposium 2002, 3: 1327-1330 (2002).
[37] Suits, G., Malila, W., Weller, T., "The Prospects for Detecting Spectral Shifts Due to Satellite Sensor Aging," Remote Sensing of Environment 26:17-29 (1988).
[38] Jakubauskas, M.E., Price, K.P., "Empirical Relationships between Structural and Spectral Factors of Yellowstone Lodgepole Pine Forests," Photogrammetric Engineering & Remote Sensing 63(12): 1375-1381 (1997).
[39] Schowengerdt, R.A., [Remote Sensing. Models and Methods for Image Processing], Academic Press, San Diego, 2. edition (2007).
[40] Perkins, T., Adler-Golden, S., Matthew, M., Berk, A., Anderson, G., Gardner, J., Felde, G., "Retrieval of Atmospheric Properties from Hyper- and Multi-Spectral Imagery with the FLAASH Atmospheric Correction Algorithm," Proceedings of SPIE: Remote Sensing of Clouds and the Atmosphere X, 5979: 59790E-1 - 59790E-11 (2005).

[41] Yokoya, N., Miyamura, N., Iwasaki, A., "Detection and correction of spectral and spatial misregistrations for hyperspectral data using phase correlation method," Applied Optics 49(24): 4568-4575 (2010).
[42] Neville, R. A., Sun, L., Staenz, K., "Detection of keystone in imaging spectrometer data," Proceedings of SPIE: Algorithms and Technologies for Multispectral, Hyperspectral and Ultraspectral Imagery X, 5425: 208-217 (2004).
[43] Pearlman, J.S., Barry, P.S., Segal, C.C., Shepanski, J., Beiso, D., Carman, S.L., "Hyperion, a Space-Based Imaging Spectrometer," IEEE Transactions on Geoscience and Remote Sensing 41(6): 1160-1173 (2003).
[44] USGS (U.S. Geological Survey), Ed.,"Website Earth Observing 1 (EO-1)," 2011 <http://eo1.usgs.gov/> (10.11.2012)
[45] Barry, P.S., [EO-1/ Hyperion Science Data User's Guide, Level 1_B], TRW Space, Defense & Information Systems, Redondo Beach, CA (2001).
[46] Bindschadler, R., Choi, H., "Characterizing and correcting Hyperion detectors using ice-sheet images," IEEE Transactions on Geoscience and Remote Sensing 41(6): 1189-1193 (2003).
[47] White, D., "Hyperion Tools 2.0 Installation and User Guide," 2011, <http://www.exelisvis.com/Default.aspx?tabid=1540&id=1163> (05.10.2012).
[48] ERDAS Inc., Ed., [ERDAS Field Guide, Fifth Edition, Revised and Expanded], Atlanta, Georgia, (1999).
[49] Pande-Chhetri, R., Abd-Elrahman, A., "De-striping hyperspectral imagery using wavelet transform and adaptive frequency domain filtering," ISPRS Journal of Photogrammetry and Remote Sensing 66: 620-636 (2011).
[50] Pande-Chhetri, R., Abd-Elrahman, A., "Filtering high-resolution hyperspectral imagery in a maximum noise fraction transform domain using wavelet-based de-striping," International Journal of Remote Sensing 34(6): 2216-2235 (2012).